Hindawi
International Journal of RF and Microwave Computer-Aided Engineering
Volume 2024, Article ID 9940203, 11 pages
https://doi.org/10.1155/2024/9940203

Research Article

A Multifunctionality Reconfigurable HMSIW Filter by Using EBG Structure and Diodes for C/X-Band Application

Kioumars Pedram and Sanghoon Sim

School of Electronics Engineering, Chungbuk National University, Cheongju, Republic of Korea

Correspondence should be addressed to Sanghoon Sim; shsim@chungbuk.ac.kr

Received 28 November 2023; Revised 14 March 2024; Accepted 22 March 2024; Published 2 April 2024

Academic Editor: Jin Xu

This letter presents a multifunctionality reconfigurable substrate-integrated waveguide (SIW) filter embedded in a microstrip line. The proposed filter used an electromagnetic bandgap structure (EBG) to compact the size and improve the electromagnetic features. The SIW filter consists of a three-cell EBG with metallic circular-shaped connected to the ground through cylindrical vias. Firstly, the base SIW structure offers a wide passband filtering response, and then, to obtain selective passband, wide band rejection, and controllable resonance frequencies, a three-cell EBG along with four diodes has been attached. The filter is designed and printed on a Rogers 4003 substrate with a thickness of 1 mm and is experimentally validated for functionalities operated at three modes with an average 3 dB bandwidth of 115 MHz in each frequency. In addition to that, two transmission zeros (TZ) have been produced in the upper band frequency. The filter's response is also tunable by turning the diode off or on and changing the main parameters of EBG, the gab, and the position between cells. The study explores resonance frequency alterations in a three-state system of on/off. By eliminating or diminishing specific modes, and incorporating diodes, distinct resonance behaviors are observed. Moreover, shifting frequency resonance in a multiparameter system has been investigated. Increasing *B1* induces a significant shift to lower values, while an increase in *D1* leads to a decrease in the first and second resonance frequencies and an upward shift in the third. The designed filter has been fabricated and tested to compare and confirm simulated responses. Simulation and measurement results are in good agreement. The S-parameters of measured results gained a good response (>15 dB) within the passbands and stopbands and an insertion loss of 1.5 dB suitable for 5G and Wi-Fi systems.

1. Introduction

Although high-performance and high-quality factors make the conventional waveguide the best choice for different communication systems, the size of these waveguides does not provide compatible circumstance to be integrated into the printed circuit board because of their bulky nature [1]. Fabrication is another big challenge for these waveguides. Therefore, to overcome this issue, recently, new technologies have gone hand in hand with improving conventional methods and structures [2]. Scientists have conducted ample studies to determine new ways to improve functionalities, electromagnetically or physically. In communication and telecommunication, due to the various frequency bands, skipping and recognizing undesired frequencies from desired ones is a vital key [3]. Meeting the requirement of communication systems acquire mixing methods along with new technologies or to name a few surface acoustic wave (SAW), substrate-integrated waveguide (SIW), and electromagnetic bandgap (EBG) structures [4]. The SIW as an adaptive technology offers lightweight and high performance for innovations in various types of applications, especially for high frequency and microwave [5]. Bandpass and stopband filters with compact sizes and low profiles working at high frequencies are attractive to satisfy the advance of next-generation wireless communication to come [6].

Since SIW filters are suitable for high-frequency applications. They can handle and shift bands by mitigating the coupling between their resonators. However, worse insertion loss and limitation of impedance matching are a worse part of SIW; it is easily utilized with other structures. Bandpass filters

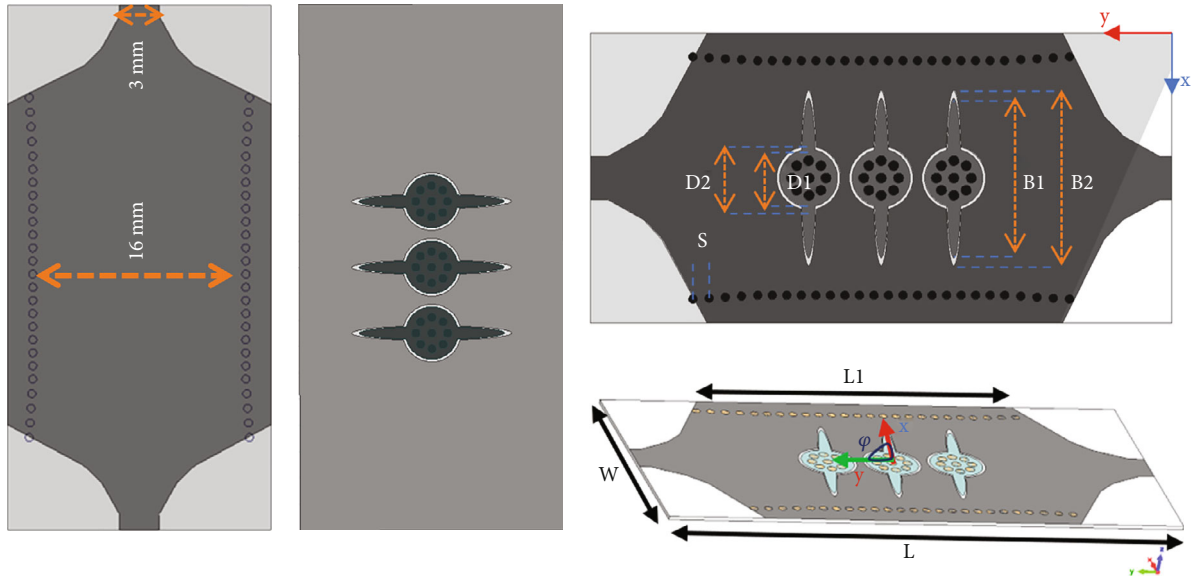

Figure 1: 3D schematic and the shape of the base form and proposed filter. (a) Basic SIW filter, (b) the bottom layer of the proposed filter, and (c) top layer and 3D view of the proposed filter.

with wide stopbands were achieved [7]. Multiband and configuration filters were introduced to obtain a flexible response and adjust its center frequencies [8–11]; moreover, it was combined with the electronically controlled dielectric constant of liquid crystal materials [12], and it was also tunable by using RF-MEMS [13] and diodes [14]. Reducing the size of the SIW structure was obtained by using metamaterial resonators [15, 16] or half-mode substrate-integrated waveguide (HMSIW) technology [17]. It miniaturizes the width of conventional SIW. Compared to similar SIW filters, it has not only decreased the overall design size but also enhanced performance [18].

On the other hand, as SIW creates high order harmonics and has an impact on out-of-band performance, electromagnetic bandgap (EBG) structures have absorbed a lot of attention in these years due to their high Qu, compatibility with other components, and low profile; therefore, EBG structures should be come in handy and suppress those issues [19, 20]. To reject out-of-band and harmonics, EBG structures illustrate very effective properties at high frequencies along with their other features such as reduced size which make them top-list for being applied in filtering [21, 22]. Out-of-band rejection capability of EBG structures has assisted in widening the filter's stopband and improving the band-to-band isolation in the filter [23, 24]. Considerable resources have been dedicated to the advancement of adjustable elements utilizing technologies like tunable microwave filters.

Semiconductor varactors, including p-i-n and varactor diodes, provide adjustable junction capacitance through the application of reverse voltage. An engineered substrate enhanced with ferromagnetic material offers an additional complementary avenue in the realm of intelligent substrate materials, granting greater flexibility in crafting tunable filters with heightened performance capabilities [25].

This designed filter has been developed using conventional SIW loaded with three cells of EBG structure equal dimensions on the bottom and top of the metallic cavity to produce a compact HMSIW filter with a multiefficient response and become adjustable and reconfigurable by inserting PIN and Zener diodes. A compact design of an HMSIW-based filter is presented to achieve the controllability issue's goal functionalities while mitigating size. The proposed multimode SIW filter has been simulated using electromagnetic (EM) Ansys high-frequency structure simulator (Ansys HFSS and CST) software; moreover, circuit-model simulated results have also been presented. Smaller size, multi fractions, fairly good return loss, and low insertion loss make the filter suitable for 5G and Wi-Fi systems.

Table 1: Dimension of the parameters of designed filter.

Parameters	
W	20 mm
L	40 mm
L1	25 mm
S	1 mm
R of via	0.3 mm
Gap	0.125 mm
D1	3 mm
D2	3 mm + 0.5 mm
B1	11 mm
B2	11 mm + 0.2 mm
Phi	10°

2. The Filter Geometry and Design Procedure

The geometry of the proposed SIW filter with three cells of EBG on a single square cavity is demonstrated in Figures 1(b) and 1(c); in addition, the definition of parameters

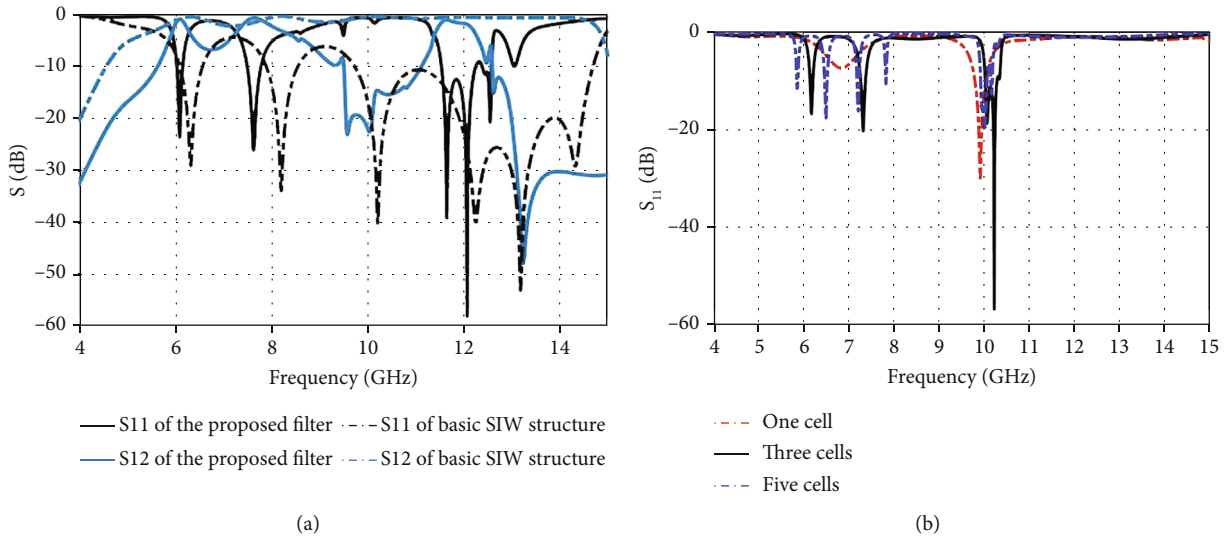

FIGURE 2: (a) Simulated S-parameter of the base form and proposed filter and (b) simulated S-parameter of three states of the proposed filter with one, three, and five cells.

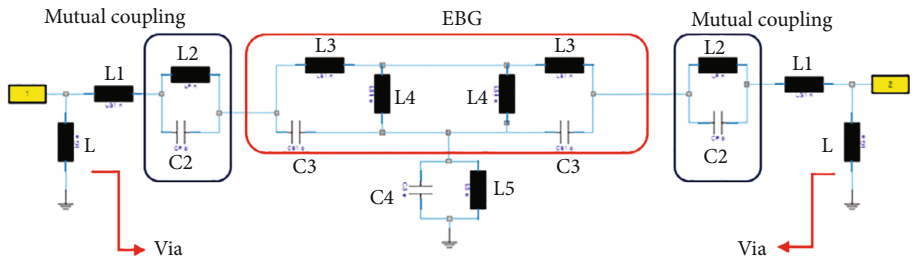

FIGURE 3: The circuit-model simulation of the proposed filter.

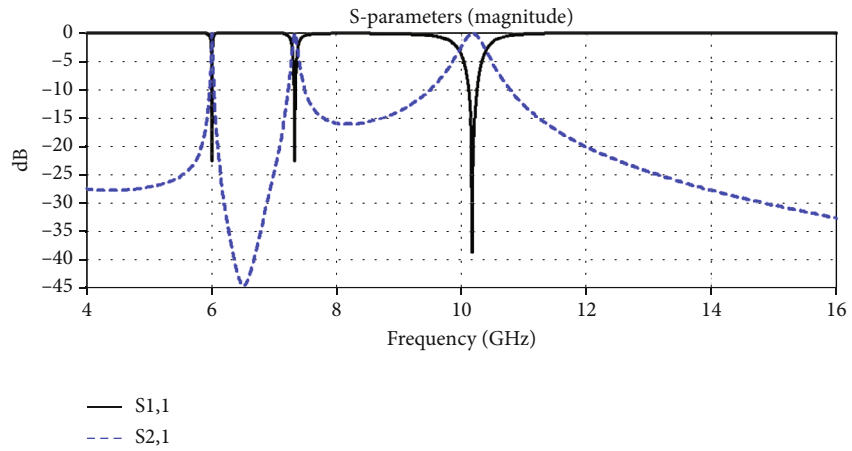

FIGURE 4: The simulated results of the circuit model of the proposed filter.

and dimensions is illustrated in Figure 1(c) and Table 1. The primary sizes of the cavity in Figure 1(b) can be obtained by the following formulas (1) and (2), where f is the resonant frequency of the cavity [26, 27];

$$f = \frac{c}{2 \times w_{\text{eff}} \sqrt{\varepsilon_r}}, \tag{1}$$

$$W_{\text{eff}} = w - \frac{d^2}{s \times 0.95}, \tag{2}$$

$$s \le 2 \times d, \quad 0.5s \le d \le 0.1\lambda_0. \tag{3}$$

To decrease dispersion loss and energy leakage, the cavity should follow two conditions in (3). d and s are the diameter

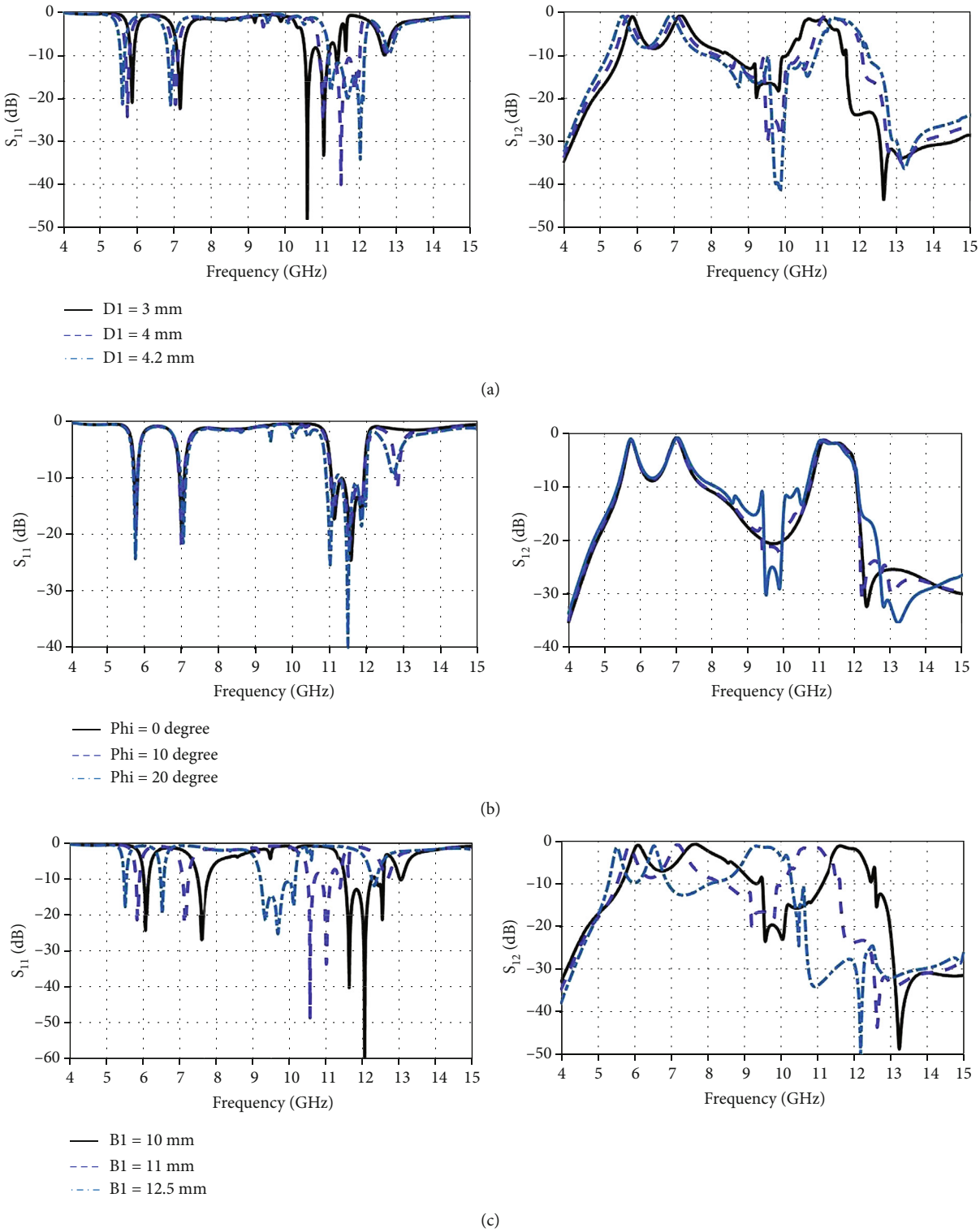

FIGURE 5: S-parameters for different values of (a) the diameter of the inside circle (D1), (b) the Phi angle (φ) from the positive x-axis to the orthogonal vector onto the X-Y plane (Phi), and (c) the length of the rectangles (B1).

and spacing between vias, respectively. ε_r is the relative dielectric constant of the chosen substrate, and w is the width of the cavity, around 16 mm. The tapered segment attaches a 50 Ω microstrip signal line to the filter. The taper is utilized by gaining well impedance matching [28].

The basic structure of the SIW filter has been designed through a rectangular cavity that links the top and the bottom metal layers which are shown in Figure 1. In the first step, the SIW rectangular cavity ($L1 \times w$) is cultivated on the RT/Duroid 4003 substrate with the thickness of 1 mm

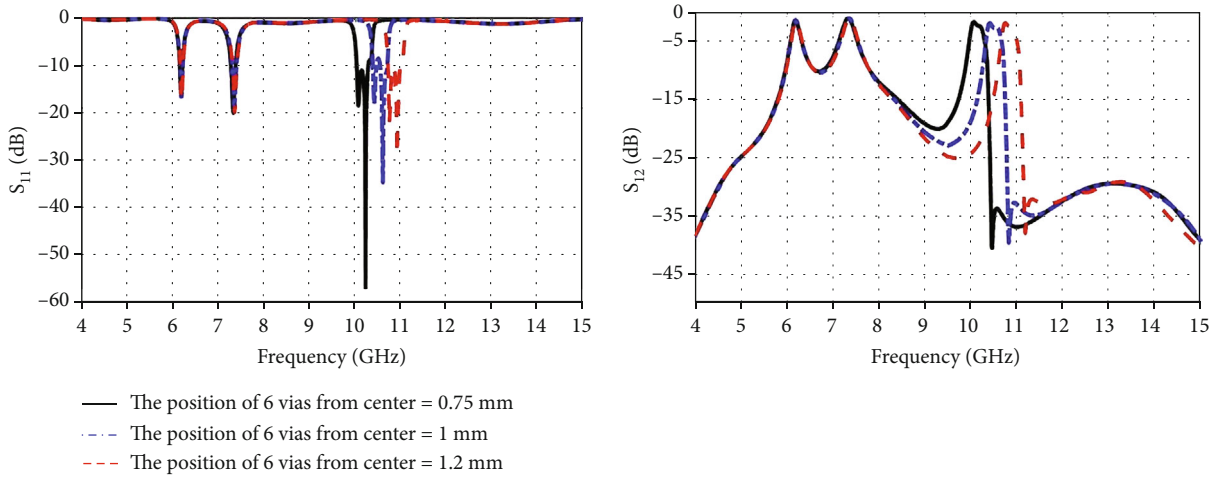

Figure 6: S-parameters for different values of the position of set vias in the middle of the structure.

having $\varepsilon_r = 3.55$ and $\tan\delta = 0.002$, and then, electromagnetic bandgap (EBG) structures are utilized and added. The basic filter results are enhanced and developed, and EBG structures are based on periodic or quasiperiodic patterns performing better in high frequency like SIW structures [29].

The EBG works the same as the phenomena of photonic bandgap (PBG) in optics. it has been imposed on microwave planar waveguides to obtain results in pass or stop bands. Nonetheless, fabrication has been still a vital issue depending on the number of vias, the size of EBG, and the locations of EBG. In mushroom-like EBG, vias play a main role in achieving stop band frequency. The prime type of EBG is like a 3D mushroom including solid patches with cylindrical vias, having an influence on the return loss and insertion loss. The size of the patch, the diameter of the vias and the gap between the unit elements, the thickness of the substrate, and the substrate material type are the key characteristics that should be considered.

Figure 2 illustrates the simulation results of the proposed and base-form filter obtained by 3D electromagnetic (EM) simulation software, Ansys HFSS. From the illustration, it was noticed that the passband frequency of the base-form filter achieves a narrow bandwidth in the C-band at 6.2 GHz from 6 GHz to 6.4 GHz as well as a wide passband covering the X-band. After adding the EBG structures, the results are restricted around $f = 6.1$ GHz, 7.33 GHz, 11.8 GHz, and 12.1 GHz, and two transmission zeros are created at around 10 GHz and 13 GHz. In other words, changing the center frequencies and transmission zeros are able to be controlled by changing the main parameters which are aforementioned before. After optimizing the structure and parametric study, the proposed filter was achieved. The improved dimension is presented in Table 1.

The filter is simulated in 3 states: one cell, three cells, and five cells of EBG. From Figure 2(b), it is interpreted that in the basic form, filter passed the 80 percent of the X-band and 20 percent of the C-band. By adding EBG cells, special resonance frequencies have been achieved in each state. By the way, for the 5 cells added to the filter, 4 frequencies have been resonated around each at C-band. Therefore, they are affected and interfere with each other. Among all of them, the proposed filter with three cells is easily controllable.

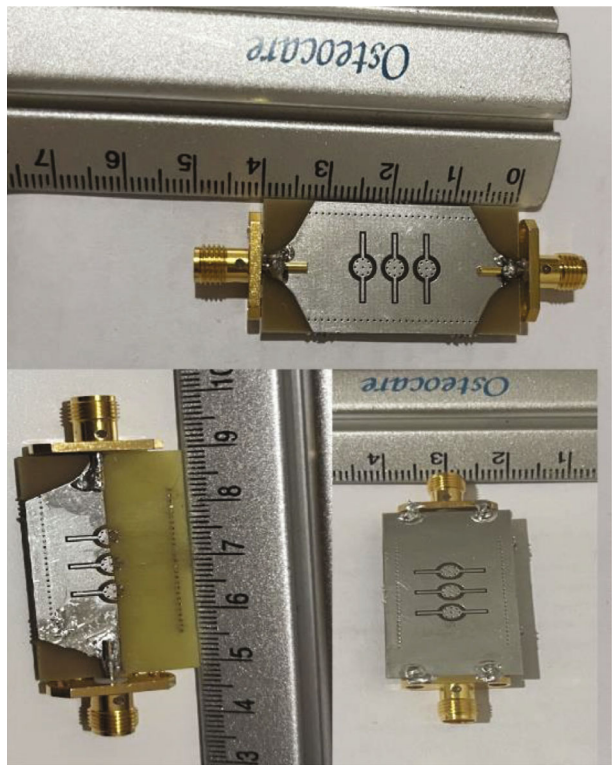

Figure 7: Fabricated structure, top and bottom view of the SIW and half-mode filter.

Figure 3 shows a basic-type EBG and its equivalent circuit model. For this type of EBG, the value of capacitance "C" and inductance "L" is given by (4) and (5), respectively [3, 4].

$$C = \frac{W\varepsilon_0(1+\varepsilon_r)}{\pi}\frac{W+g}{g}\Bigg), \tag{4}$$

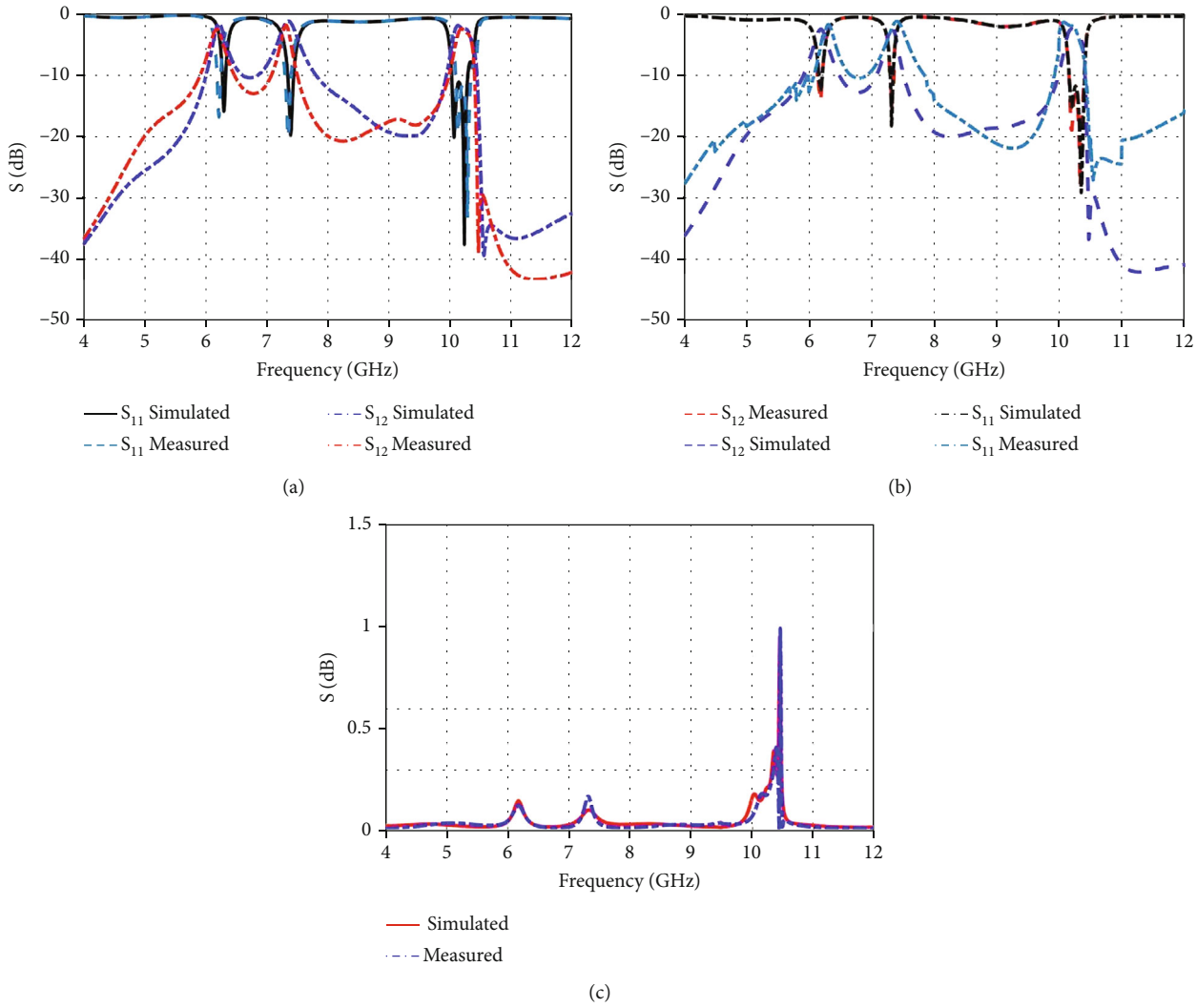

FIGURE 8: Simulated and fabricated results of return loss and insertion loss of (a) SIW filter and (b) half-mode SIW filter and (c) the simulated and measured results of group delay of SIW filter.

$$L = 2 \times 10^{-7} h \left[\frac{2h}{r} \right) + 0.5 \left(\frac{2r}{h} \right) - 0.75 \Bigg]. \quad (5)$$

Here, "W" is the side length of the patch, "g" is the gap between units, "h" is the thickness of the substrate, "r" is the radius of the vias, ε_0 is the permittivity of free space, and ε_r is relative permittivity.

An LC filter is able to be utilized for the description of the performance of the EBG structure. The current distributing around vias causes the inductor, while the gap between the cells patches results in the capacitor. The LC model of a combination of EBG and SIW structure is illustrated in Figure 3 which provides the circuit principal level analysis. The EBG with three cells and SIW structure with via-hole walls on both sides of the EBG structure can be replaced by the group of L and C components as inductances and capacitances in a circuit model in Figure 3. Since having a coupling between EBG units and both structures, L2, C2, L5, and C4 are represented as the mutual coupling between them. By changing the value of the parameters, the resonating frequency can be improved. Actually, the values of each parameter for the proposed equivalent circuit model for the filter are calculated and simulated in CST Studio Suite 3D EM simulation and analysis software. It ends up with $L = 0.9$nH, $L1 = 3.9$nH, $C2 = 2$pF, $L2 = 2$nH, $C3 = 1.3$pF, $L3 = 0.4$nH, $C4 = 0.41$pF, $L4 = 0.9$nH, and $L5 = 0.18$nH. Figure 4 shows the circuit-model simulation and whose results, the three modes of the developed filter, are well achieved; moreover, the results are the same as the simulation.

3. Parametric Study

Some selective and effective parameters are selected to clarify the parametric study so as to have a better comprehension of the results. The main keys are to obtain return loss and insertion loss results [30]. Parametric studies of the filter have been conducted to investigate the way how the filtering response is behaving. S-parameters' responses of the different values of D1, Phi, and B1 are indicated in

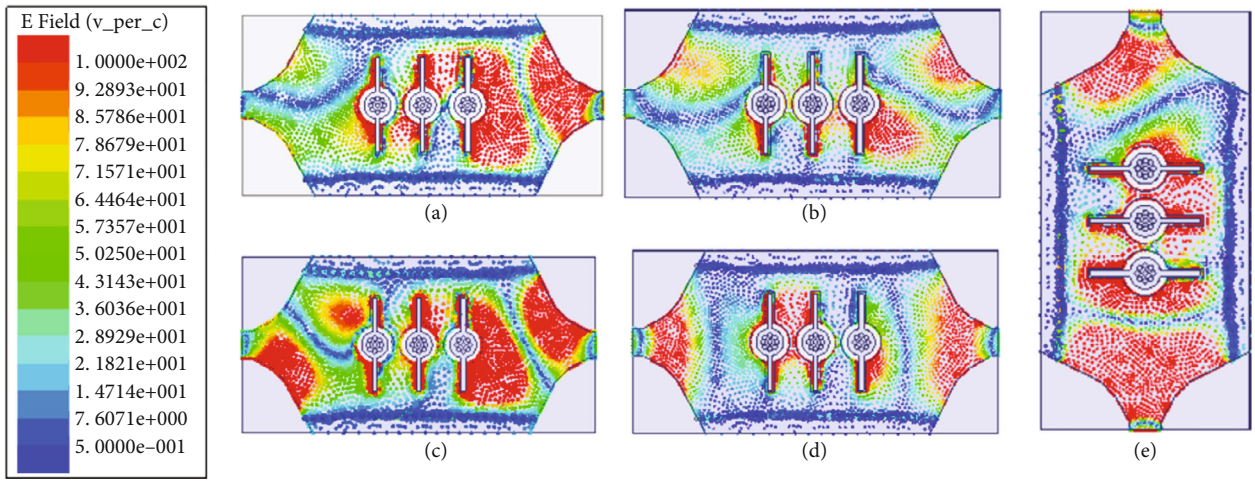

Figure 9: Simulation of electric-field distributions of two transmission zeros at (a) 10.45 GHz and (b) 9.3 GHz and simulation of electric-field distributions of three modes at (c) 6.19 GHz, (d) 7.33 GHz, and (e) 10.22 GHz.

Figures 5(a)–5(c). From the illustration, it resulted that the third mode high frequency by varying the parameter D1 from 3 to 4.2 mm has been affected more than other modes. The position of the first and second bands mildly changes around the center frequency. Analogously, the S-parameters response in different values of B1 is shown in Figure 5. The illustration showed that by varying B1 from 10 to 12.5 mm, the resonance frequencies of the three modes are shifted toward the lower frequency. Whereas S-parameters remained unchangeable by changing Phi from 0 to 20, just stopband and S-parameter responses have been improved. As it is seen from the illustration in Figure 6, the third mode depends on the position of six via in the center of structure. In other words, it can be controlled through changing the position from 0.75 to 1.2. Finally, the value of 0.75 has been selected because of its good result of return loss and insertion loss.

4. Fabricated Filters and Measured Results

The SIW and half-mode SIW using EBG structures have been successfully simulated and fabricated, so the prototype of the fabricated filter has been illustrated in Figure 7. Based on the rectangular waveguide theory, design rules of SIW for obtaining an effective via-hole array and reducing the width of the broad sidewall were examined. HMSIW not only minimizes the size of the structure but also upholds all the features of the SIW [31]. Based on the results in Figures 8(a) and 8(b), it was illustrated that the cut-off frequencies are not varied, and return loss and insertion loss show good results.

For experimental verification, the SIW filter used three-cell EBG that has been fabricated and tested. The results are the same as the simulated results, including four center frequencies at 6.19 GHz, 7.33 GHz, and 10.22 GHz and two transmission zeros at 9.3 GHz and 10.45 GHz. The experimental validation has been done by vector network analyzer. Figures 8(a) and 8(b) depict the simulated and measured performances of the designed filter. According to the graph,

Table 2: The different state of diodes.

	Diode 1	Diode 2	Diode 3	Diode 4
First state	Off	Off	On	Off
Second state	Off	Off	Off	On
Third state	On	On	On	On

it can be shown that the measured results show a passband with an average bandwidth of 115 MHz at each resonance. The measured 10 dB upper band rejection and lower band rejection with two transmissions zero have been achieved. The measured results of S-parameters admit a good return loss and insertion loss of the resonance frequencies, greater than 17 and 1 dB, respectively. Two transmission zeros have been created in the upper band frequency. Based on the curve, it has been found that there are slight shifts and changes in results when compared with the simulated one.

Another key factor in a filter is the group delay which should be constant in an ideal state [31]. The group delay of the designed filter is indicated in Figure 8(c). From the illustration, the simulated and measured result is about 1 ns at the lower and upper edges of the passband; moreover, it obtains a nice response at the whole passband, and it can be seen that the group delay of the designed filter is about constant. A crucial aspect in filter design involves determining the roll-off factor, which denotes the rate of transition from passband to stopband. The calculation of this parameter is facilitated by employing the equation presented in reference [32].

$$\text{Roll-off} = \frac{\alpha_{\max} - \alpha_{\min}}{f_s - f_c}\left(\frac{\text{dB}}{\text{GHz}}\right). \tag{6}$$

Within this expression, $\alpha_{\max}$ typically assumes a value of -40 dB, while $\alpha_{\min}$ is set at -3 dB. Here, f_s represents the frequency corresponding to the -40 dB point, and f_c denotes the cut-off frequency. The proposed SIW filter features a

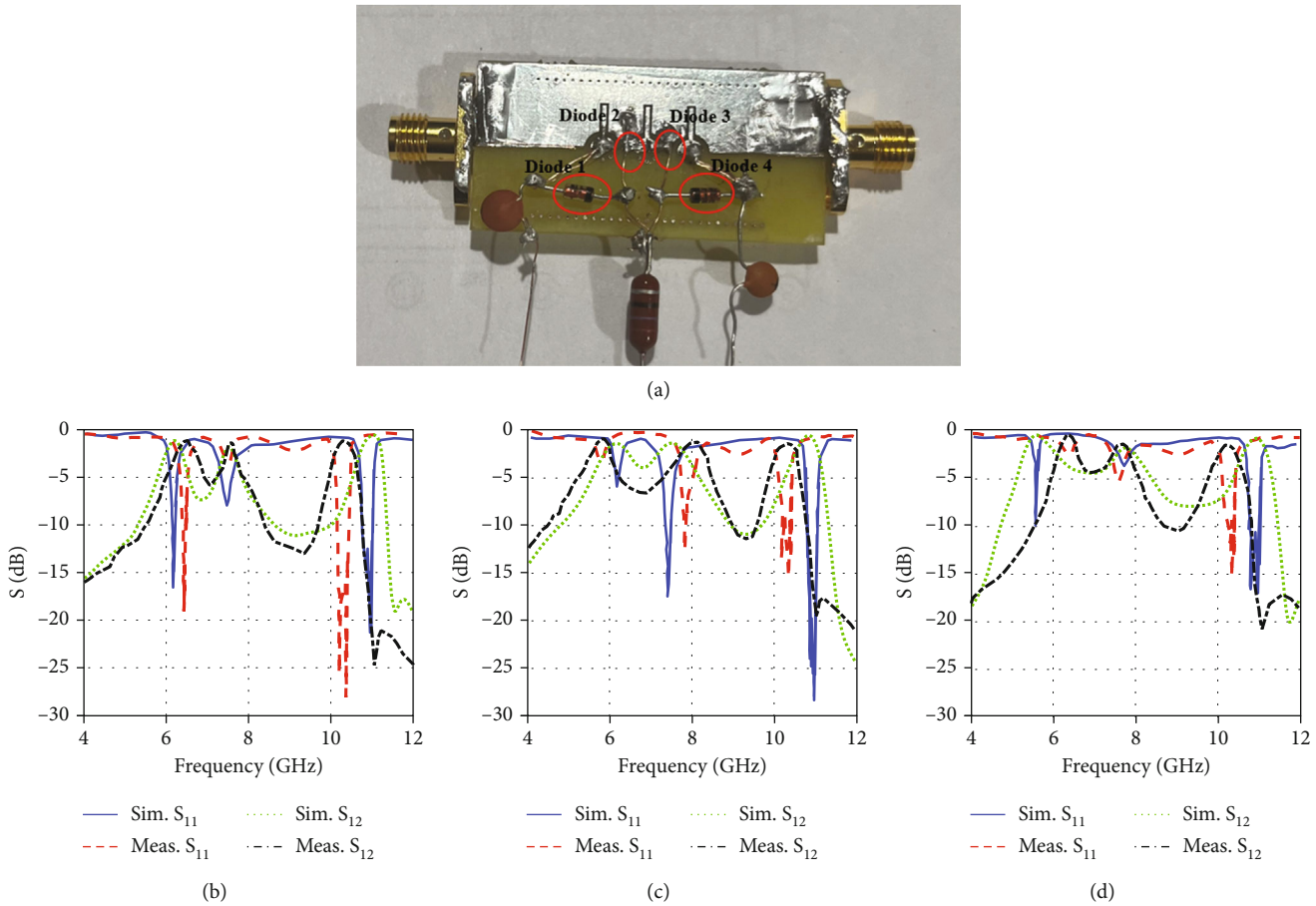

FIGURE 10: (a) Photograph of the fully reconfigurable filter using three resonant cells and four diodes and simulated and measured results (S_{11} and S_{12}) of (b) first state, (c) second state, and (d) third state.

transition band spanning 0.7 GHz, ranging from 9.8 to 10.5 GHz, accompanied by attenuation levels of -3 dB and -40 dB, respectively. Additionally, the half-mode SIW filter under consideration has a transition band covering 0.9 GHz, extending from 10 to 10.9 GHz, with corresponding attenuation levels of -3 dB and -40 dB, respectively. The figure illustrates a roll-off parameter of 52.8 dB/GHz for the SIW structure and 41.1 dB/GHz for the half-mode SIW structure.

5. Electric-Field Distribution

To verify the performance of the designed filter, the simulated electric-field distributions at various frequencies are illustrated in Figure 9. According to the illustrations, after applying transmission zero frequency at 10.45 GHz and 9.3 GHz, the electromagnetic (EM) waves fail to propagate through the structures to the output port. On the other hand, in the three modes, the EM waves manage to propagate easily, based on the results. It can also be recognized that the electric fields are highly concentrated around three cells of EBG structures. Their electric-field distributions across the cross-sections at the resonance's frequency of 10.22, 7.33, 6.19 GHz are depicted in Figure 9.

6. Reconfigurable Simulation and Measurement Results

In order to verify reconfigurable features, the simulated and measured return/insertion losses of the designed reconfigurable filter have been obtained, and three main states have been examined in terms of Table 2. Figure 10 shows the simulated performance; the selective mode is determined by turning the diode state on the top of the filter connecting three cells of EBG to each other. Three states of the filter are shown in Table 2. As is seen in Figure 10, in the first state, mode 1 has been removed, and others remain unchanged; while in the second one, the second mode has faded away, and both modes have been unchanged. From the simulation, the third state offers just the third mode and cuts down others. Imparting the diodes into the structure alters the resonance frequencies; moreover, because of uncontrolled conditions and experimental error, they have been slightly shifted, according to the measured results shown in Figure 10.

The presented filter consists of three diodes. Two Zener diodes (1N4733) and two PIN diodes (SMP) are placed between the cells to obtain the reconfigurability function. To confirm the design concept, workable PIN diodes were utilized with a size of $1.5 \times 0.5\,\text{mm}^2$, as switches. In the

Table 3: Comparison of the designed filter with previous literature.

	Size (mm^2)	Substrate	Technique	CF (GHz)	TZ (GHz)	IL (dB)	3 dB FBW (MHz)	Number of modes	Number of TZ
[5]	17.5×42	Rogers RT/Duroid 5880	SIW SSPP	—	—	1	5500	1	—
[20]	9×50	Rogers 4350	Microstrip SIW CSRR	4.67	8.1 10.5	1	3100	1	2
[26]	31.35×28.2	Rogers RT/Duroid 5880	Microstrip SIW	8.05 9.99	—	1.74 2.21	400 300	2	4
[27]	11×21.9	Rogers RT/Duroid 5880	RSIW	16 27	—	0.7 2.5	300 200	3	—
[28]	38.5×37.5	Rogers 4350B	SIW	8.5	7.8 8.9 10.4	1.7	520	1	3
[33]	22×26	Rogers RT/Duroid 5870	SIW	1.5 4.96	2.9 7.12	0.85 0.9	300 400	2	2
[34]	49×77	Rogers 4003	Circular SIW	5.6	6.2	1.1	250	3	1
[35]	$0.85\lambda^2$	Rogers RT/Duroid 5870	SIW	6.2 7.75	5.80 9.8	0.87 0.75	250 340	—	2
This work	8×40	Rogers 4003	SIW and EBG HSIW and EBG	6.19 7.33 10.22	9.3 10.45	1.85 1.25 1.5	100 100 300	3	2

CF: center frequency; TZ: transmission zero; IL: insertion loss; FBW: frequency bandwidth.

computer simulation program, HFSS, these diodes were simulated with a lumped element given almost 1.5 as the resistance value of the PIN diode in the on state and almost 0.2 pF as the capacitance value in the off state. In the off mode, a PIN diode is simulated as a series capacitance along with a parasitic inductance. In the on mode, a PIN diode is replaced with a series resistance and a parasitic inductance. The PIN diodes are planned for applications from 10 MHz to more than 10 GHz.

7. Comparison

Table 3 examines and comprises the performance of the designed filters with previous articles. The filter provides versatile features and multifunctionalities in comparison with other preferences, such as occupying a smaller area, obtaining low insertion loss, and good return loss as well as having two transmission zeros along three modes. The designed filter with Rogers 4003 is lightweight, low profile, and low cost; in addition, it achieves a low insertion loss and a better return loss. The result of the equivalent circuit model has verified the full-wave simulation response for the designed filter. The proposed filter with three numbers of resonance frequencies and two transmission zeros provides strong operation in the passband and out-of-band rather than the previous works. Compared with others, the proposed filter also offers a size reduction of 40%.

8. Conclusion

The design and analysis of a compact HMSIW filter using the EBG structure and electronic devices have been presented. The designed filter is loaded with a three-cell EBG with metallic circular-shaped connected to the ground through cylindrical vias to achieve several resonance frequencies and transmission zeros, wide lower and upper bands of rejection. The working frequencies of the filter are shifted by changing the EBG parameters and are tunable by turning off and on all diodes in 3 states. The HMSIW filter has been simulated, fabricated, and tested. The measured results and the simulated results are analogous together. It covers average 115 MHz bandwidth at each of the center frequencies of 6.19 GHz, 7.33 GHz, and 10.22 GHz and has two transmission zeros at 9.3 GHz and 10.45 GHz. The measured results are greater than 17 in return loss and 1.5 dB in insertion loss. The low-cost and low-profile filter is tunable and convenient for 5G and Wi-Fi systems.

Data Availability

The data that support the findings of this study are available from the authors upon reasonable request.

Conflicts of Interest

The authors declare that they have no conflicts of interest.

Acknowledgments

This work was supported by the research grant of the Chungbuk National University in 2022.

References

[1] M. Bozzi, A. Georgiadis, and K. Wu, "Review of substrate-integrated waveguide circuits and antennas," *IET Microwaves, Antennas & Propagation*, vol. 5, no. 8, pp. 909–920, 2011.

[2] Y. Wu, Y. Chen, L. Jiao, Y. Liu, and Z. Ghassemlooy, "Dual-band dual-mode substrate integrated waveguide filters with independently reconfigurable TE_{101} resonant mode," *Scientific Reports*, vol. 6, no. 1, article 31922, 2016.

[3] S. Moitra and P. S. Bhowmik, "Modelling and analysis of substrate integrated waveguide (SIW) and half-mode SIW (HMSIW) band-pass filter using reactive longitudinal periodic structures," *AEU - International Journal of Electronics and Communications*, vol. 70, no. 12, pp. 1593–1600, 2016.

[4] S. Shahriar-Bahramipour and K. Afrooz, "Fishbone substrate integrated waveguide structures," *AEU-International Journal of Electronics and Communications*, vol. 107, pp. 177–182, 2019.

[5] R. S. Sangam and R. S. Kshetrimayum, "Hybrid spoof surface plasmon polariton and substrate integrated waveguide bandpass filter with high out-of-band rejection for X-band applications," *IET Microwaves, Antennas & Propagation*, vol. 15, no. 3, pp. 289–299, 2021.

[6] P. Bhardwaj, S. Deivalakshmi, and R. Pandeeswari, "Compact wideband substrate integrated waveguide bandpass filter for X/Ku-bandapplication," *International Journal of RF and Microwave Computer-Aided Engineering*, vol. 31, no. 6, Article ID e22634, 2021.

[7] B. Lee, S. Nam, S.-W. Jeong, and J. Lee, "Post-loaded substrate-integrated waveguide bandpass filter with wide upper stopband and reduced electric field intensity," *IEEE Microwave and Wireless Components Letters*, vol. 30, no. 4, pp. 371–374, 2020.

[8] P. Chu, W. Hong, M. Tuo et al., "Dual-mode substrate integrated waveguide filter with flexible response," *IEEE Transactions on Microwave Theory and Techniques*, vol. 65, no. 3, pp. 824–830, 2017.

[9] X. Zhou, G. Zhang, J. Zheng et al., "Design of dual-band balanced bandpass filter based on a single substrate integrated waveguide cavity," *International Journal of RF and Microwave Computer-Aided Engineering*, vol. 32, no. 8, Article ID e23213, 2022.

[10] S.-W. Jeong, G. Lee, J. Lee, and J. Lee, "Frequency-tunable absorptive bandpass filter using substrate-integrated waveguide structure," *IEEE Transactions on Microwave Theory and Techniques*, vol. 69, no. 12, pp. 5351–5359, 2021.

[11] X. Guo, L. Zhu, and W. Wu, "Design method for multiband filters with compact configuration in substrate integrated waveguide," *IEEE Transactions on Microwave Theory and Techniques*, vol. 66, no. 6, pp. 3011–3018, 2018.

[12] D. Jiang, Y. Liu, X. Li, G. Wang, and Z. Zheng, "Tunable microwave bandpass filters with complementary split ring resonator and liquid crystal materials," *IEEE Access*, vol. 7, pp. 126265–126272, 2019.

[13] A. El Mostrah, A. Muller, J. F. Favennec et al., "An RF-MEMS-based digitally tunable SIW filter in X-band for

communication satellite applications," *Applied Sciences*, vol. 9, no. 9, p. 1838, 2019.

[14] S. Heydari, K. Pedram, Z. Ahmed, and F. B. Zarrabi, "Dual band monopole antenna based on metamaterial structure with narrowband and UWB resonances with reconfigurable quality," *AEU-International Journal of Electronics and Communications*, vol. 81, pp. 92–98, 2017.

[15] M. Danaeian and H. Ghayoumi-Zadeh, "Miniaturized substrate integrated waveguide filter using fractal open complementary split-ring resonators," *International Journal of RF and Microwave Computer-Aided Engineering*, vol. 28, no. 5, Article ID e21249, 2018.

[16] M. Danaeian, K. Afrooz, and A. Hakimi, "Miniaturization of substrate integrated waveguide filters using novel compact metamaterial unit-cells based on SIR technique," *AEU-International Journal of Electronics and Communications*, vol. 84, pp. 62–73, 2018.

[17] A. Iqbal, J. J. Tiang, C. K. Lee, N. K. Mallat, and S. W. Wong, "Dual-band half mode substrate integrated waveguide filter with independently tunable bands," *IEEE Transactions on Circuits and Systems II: Express Briefs*, vol. 67, no. 2, pp. 285–289, 2020.

[18] T. R. Jones and M. Daneshmand, "Miniaturized folded ridged half-mode and quarter-mode substrate integrated waveguides for filter design," *IEEE Transactions on Microwave Theory and Techniques*, vol. 67, no. 8, pp. 3414–3426, 2019.

[19] J. de Dios Ruiz, F. L. Martinez-Viviente, A. Alvarez-Melcon, and J. Hinojosa, "Substrate integrated waveguide (SIW) with Koch fractal electromagnetic bandgap structures (KFEBG) for bandpass filter design," *IEEE Microwave and Wireless Components Letters*, vol. 25, no. 3, pp. 160–162, 2015.

[20] L. Huang and N. Yuan, "A compact wideband SIW bandpass filter with wide stopband and high selectivity," *Electronics*, vol. 8, no. 4, p. 440, 2019.

[21] Y. Guo, H. Wang, S. Fu, S. Dou, W. Wang, and H. Wu, "Compact CEBG filter for high-frequency applications with low insertion loss," *IEEE Transactions on Components, Packaging and Manufacturing Technology*, vol. 13, no. 1, pp. 99–109, 2023.

[22] H. García-Martínez, E. Avila-Navarro, G. Torregrosa-Penalva et al., "Design and fabrication of a band-pass filter with EBG single-ridge waveguide using additive manufacturing techniques," *IEEE Transactions on Microwave Theory and Techniques*, vol. 68, no. 10, pp. 4361–4368, 2020.

[23] H. García-Martínez, G. Torregrosa-Penalva, E. Àvila-Navarro, N. Delmonte, L. Silvestri, and M. Bozzi, "3D-printed electromagnetic band-gap band-pass filter based on empty single-ridge waveguide," *IEEE Access*, vol. 10, pp. 53954–53962, 2022.

[24] J. A. Brown, S. Barth, B. P. Smyth, and A. K. Iyer, "Compact mechanically tunable microstrip bandstop filter with constant absolute bandwidth using an embedded metamaterial-based EBG," *IEEE Transactions on Microwave Theory and Techniques*, vol. 68, no. 10, pp. 4369–4380, 2020.

[25] J. Ge, T. Wang, Y. Peng, and G. Wang, "Electrically tunable microwave technologies with ferromagnetic thin film: recent advances in design techniques and applications," *IEEE Microwave Magazine*, vol. 23, no. 11, pp. 48–63, 2022.

[26] Y. Zhu and Y. Dong, "A compact dual-band quasi-elliptic filter based on hybrid SIW and microstrip technologies," *IEEE Transactions on Circuits and Systems II: Express Briefs*, vol. 69, no. 3, pp. 719–723, 2022.

[27] R. Cao, J. Y. Deng, R. M. Shang, W. Lin, and Z. Chen, "Miniaturizeddual-bandridged substrate integrated waveguide cavity resonator andband-passfilters," *International Journal of RF and Microwave Computer-Aided Engineering*, vol. 32, no. 12, Article ID e23541, 2022.

[28] W. Shen and H.-R. Zhu, "Vertically stacked trisection SIW filter with controllable transmission zeros," *IEEE Microwave and Wireless Components Letters*, vol. 30, no. 3, pp. 237–240, 2020.

[29] W. Fu, Z. Li, P. Liu, J. Cheng, and X. Qiu, "Modeling and analysis of novel CSRRs-loaded dual-band bandpass SIW filters," *IEEE Transactions on Circuits and Systems II: Express Briefs*, vol. 68, no. 7, pp. 2352–2356, 2021.

[30] H.-W. Xie, K. Zhou, C.-X. Zhou, and W. Wu, "Substrate-integrated waveguide triple-band bandpass filters using triple-mode cavities," *IEEE Transactions on Microwave Theory and Techniques*, vol. 66, no. 6, pp. 2967–2977, 2018.

[31] Y. Tang, K. Wu, and N. K. Mallat, "Development of substrate integrated waveguide filters for low-cost high-density RF and microwave circuit integration: pseudo-elliptic dual mode cavity band-pass filters," *AEU - International Journal of Electronics and Communications*, vol. 70, no. 10, pp. 1457–1466, 2016.

[32] G. Moloudian and M. Dousti, "Design and fabrication of a compact microstrip lowpass-bandpass diplexer with high isolation for telecommunication applications," *International Journal of RF and Microwave Computer-Aided Engineering*, vol. 28, no. 5, Article ID e21248, 2018.

[33] N. C. Pradhan, S. Koziel, R. K. Barik, A. Pietrenko-Dabrowska, and S. S. Karthikeyan, "Miniaturized dual-band SIW-based bandpass filters using open-loop ring resonators," *Electronics*, vol. 12, no. 18, p. 3974, 2023.

[34] N. C. Pradhan, S. Koziel, R. K. Barik, and A. Pietrenko-Dabrowska, "Bandwidth-controllable third-order band pass filter using substrate-integrated full- and semi-circular cavities," *Sensors*, vol. 23, no. 13, p. 6162, 2023.

[35] N. C. Pradhan, S. S. Karthikeyan, R. K. Barik, and Q. S. Cheng, "A novel compact diplexer employing substrate integrated waveguide loaded by triangular slots for C-band application," *Journal of Electromagnetic Waves and Applications*, vol. 36, no. 6, pp. 830–842, 2022.